# Impact of the Choice of Native $T_1$ in Pixelwise Myocardial Blood Flow Quantification

Corina Kräuter, MS,[1,2] Ursula Reiter, PhD,[1*] Clemens Reiter, MD,[1] Volha Nizhnikava, MD,[1] Albrecht Schmidt, MD,[3] Rudolf Stollberger, PhD,[2] Michael Fuchsjäger, MD,[1] and Gert Reiter, PhD[1,4]

**Background:** Quantification of myocardial blood flow (MBF) from dynamic contrast-enhanced (DCE) MRI can be performed using a signal intensity model that incorporates $T_1$ values of blood and myocardium.
**Purpose:** To assess the impact of $T_1$ values on pixelwise MBF quantification, specifically to evaluate the influence of 1) study population-averaged vs. subject-specific, 2) diastolic vs. systolic, and 3) regional vs. global myocardial $T_1$ values.
**Study Type:** Prospective.
**Subjects:** Fifteen patients with chronic coronary heart disease.
**Field Strength/Sequence:** 3T; modified Look–Locker inversion recovery for $T_1$ mapping and saturation recovery gradient echo for DCE imaging, both acquired in a mid-ventricular short-axis slice in systole and diastole.
**Assessment:** MBF was estimated using Fermi modeling and signal intensity nonlinearity correction with different $T_1$ values: study population-averaged blood and myocardial, subject-specific systolic and diastolic, and segmental $T_1$ values. Myocardial segments with perfusion deficits were identified visually from DCE series.
**Statistical Tests:** The relationships between MBF parameters derived by different methods were analyzed by Bland–Altman analysis; corresponding mean values were compared by *t*-test.
**Results:** Using subject-specific diastolic $T_1$ values, global diastolic MBF was $0.61 \pm 0.13$ mL/(min·g). It did not differ from global MBF derived from the study population-averaged $T_1$ ($P = 0.88$), but the standard deviation of differences was large (0.07 mL/(min·g), 11% of mean MBF). Global diastolic and systolic MBF did not differ ($P = 0.12$), whereas global diastolic MBF using systolic ($0.62 \pm 0.13$ mL/(min·g)) and diastolic $T_1$ values differed ($P < 0.05$). If regional instead of global $T_1$ values were used, segmental MBF was lower in segments with perfusion deficits (bias = −0.03 mL/(min·g), −7% of mean MBF, $P < 0.05$) but higher in segments without perfusion deficits (bias = 0.01 mL/(min·g), 1% of mean MBF, $P < 0.05$).
**Data Conclusion:** Whereas cardiac phase-specific $T_1$ values have a minor impact on MBF estimates, subject-specific and myocardial segment-specific $T_1$ values substantially affect MBF quantification.
**Level of Evidence:** 3
**Technical Efficacy Stage:** 3

J. MAGN. RESON. IMAGING 2021;53:755–765.

DYNAMIC CONTRAST-ENHANCED (DCE) cardiac magnetic resonance imaging (MRI) represents a recognized technique for the assessment of myocardial perfusion and ischemia.[1,2] Whereas a series of longitudinal relaxation time ($T_1$)-weighted images acquired during the first passage of a bolus of contrast agent (CA) are typically inspected visually for regional myocardial perfusion deficits, corresponding temporal signal intensity

View this article online at wileyonlinelibrary.com. DOI: 10.1002/jmri.27375

Received Jun 17, 2020, Accepted for publication Sep 8, 2020.

*Address reprint requests to: U.R., Division of General Radiology, Department of Radiology, Medical University of Graz, Auenbruggerplatz 9/P, A-8036 Graz, Austria. E-mail: ursula.reiter@medunigraz.at

From the [1]Division of General Radiology, Department of Radiology, Medical University of Graz, Graz, Austria; [2]Institute of Medical Engineering, Graz University of Technology, Graz, Austria; [3]Division of Cardiology, Department of Internal Medicine, Medical University of Graz, Graz, Austria; and [4]Research and Development, Siemens Healthcare Diagnostics GmbH, Graz, Austria

Additional supporting information may be found in the online version of this article

(SI) changes might be employed not only to derive semiquantitative perfusion-related parameters but also to estimate quantitative myocardial blood flow (MBF) in units of mL/(min·g).[3,4]

MBF relates temporal CA concentration changes in the left ventricular (LV) blood pool, represented by the arterial input function (AIF), with temporal CA concentration changes in myocardial tissue.[3,4] Consequently, MBF estimation requires the conversion of measured SI in blood and myocardial tissue into corresponding CA concentrations, which is complicated by their typically nonlinear relationships.[4,5] Various conversion methods have been introduced, including minimization of deviation from linearity directly during image acquisition, as performed by low-dosage, dual-bolus, and dual-sequence approaches, the use of retrospectively empirical calibration curves, or the application of SI models in combination with additional calibration images.[6–14]

The usage of an SI model that incorporates native $T_1$ values of blood and myocardium for SI-to-CA-concentration conversion is tempting because of its universality and the integration of $T_1$ mapping into clinical cardiovascular MRI.[15] While MBF estimation has been extensively studied employing native $T_1$ normal values, the first attempts were made to render the method more subject-specific by using native blood and myocardial $T_1$ values measured from native $T_1$ maps.[14,16–21] The feasibility of pixelwise MBF quantification employing an SI model incorporating native $T_1$ values of blood and myocardium remains, however, to be examined. Studies show that native myocardial $T_1$ values differ between systole and diastole as well as between myocardial segments, the latter especially if infarcted regions are present.[22–24] We therefore hypothesize that not only global, but also regional native myocardial $T_1$ values, as well as the cardiac phase of native $T_1$ maps, affect SI model-based MBF estimates.

Thus, the aims of this study were to assess the impact of native $T_1$ values on pixelwise MBF quantification by evaluating 1) the necessity for using subject-specific native $T_1$ values, 2) the influence of the cardiac phase, and 3) the need for using regional instead of global native myocardial $T_1$ values.

## Materials and Methods

### Study Population

This prospective study (ClinicalTrials.gov identifier, NCT03253835) was approved by the local Ethical Review Board, and all subjects gave written informed consent. Between February 2016 and April 2017, 20 adult patients with known chronic coronary heart disease (CHD) and without contraindications to contrast-enhanced MR underwent comprehensive cardiac MRI including myocardial DCE imaging and native and postcontrast $T_1$ mapping. To allow clear assignment of DCE series and $T_1$ maps to a cardiac phase, five subjects were excluded from analysis because of arrhythmia or erroneous electrocardiographical (ECG) triggering during DCE imaging or $T_1$ mapping. Thus, the analyzed patient population consisted of 15 patients (13 male, 2 female).

### MR Image Acquisition

ECG-gated cardiac MR was performed with a 3T clinical MR scanner (Magnetom Skyra, Siemens Healthcare, Erlangen, Germany) using an 18-channel body coil and 12 elements of a 32-channel spine coil with the patient in the supine position. $T_1$ maps and DCE series were acquired under a resting condition and inspiratory breath-holding in the same mid-ventricular short-axis slice.

An ECG-gated modified Look–Locker inversion recovery (MOLLI) sequence with single-shot balanced steady-state free precession (bSSFP) readout, motion correction, and automatic $T_1$ map generation was used to derive native $T_1$ maps at end-systole and diastasis. The MOLLI scheme was 5(5)3, meaning the acquisition of five images after the first inversion pulse and after a waiting period of five heartbeats the acquisition of three further images after a second inversion pulse.[25,26] Protocol parameters of the bSSFP readout were repetition time (TR) = 2.7 msec; echo time (TE) = 1.1 msec; flip angle = 35°; bandwidth = 1085 Hz/pixel; generalized autocalibrating partially parallel acquisition (GRAPPA) factor = 2; partial Fourier reconstruction = 7/8; field of view (FOV) = 307 × 360 $mm^2$; and voxel size = 2.1 × 1.4 × 8.0 $mm^3$.

DCE imaging was performed with the CA gadobutrol (Gadovist, Bayer Schering Pharma, Berlin, Germany) at a dose of 0.05 mmol/kg body weight. The CA was administered into the right antecubital vein by means of a power injector (Medrad, Volkach, Germany) at a rate of 4 mL/s, followed by a saline flush of 30 mL at the same rate. Starting with CA administration, its passage was imaged for 70 heartbeats employing an ECG-gated single-shot saturation recovery fast low-angle shot (SR FLASH) sequence; the breath-hold command given during acquisition targeted a breath-hold period from the arrival of the bolus in the LV until its second pass. The imaging time per frame of the SR FLASH sequence was 158.8 msec, which allowed imaging of the same mid-ventricular short-axis slice four to six times within each cardiac interval. Further protocol parameters were TR = 2.2 msec; TE = 1.1 msec; time between composite saturation pulse and central *k*-space line of image readout (TI) = 90 msec; flip angle = 12°; bandwidth = 930 Hz/pixel; GRAPPA factor = 2; FOV = 330 × 360 $mm^2$; voxel size = 2.7 × 1.9 × .0 $mm^3$; and matrix = 124 × 192. Images of the DCE scan within the first two heartbeats were acquired without applying magnetization preparation at a low flip angle of 5°. The resulting (precontrast) proton density-weighted images were used to estimate the coil sensitivity of the receiver coils. This estimation, together with a surface coil correction as well as a nonrigid motion correction of every frame, was performed automatically during image reconstruction by the scanner software.[27]

Immediately after the DCE scan, a second bolus of CA was administered at a dose of 0.10 mmol/kg body weight. Approximately 15 minutes after CA administration, myocardial late gadolinium enhancement (LGE) was imaged by $T_1$ mapping at diastasis employing the MOLLI sequence described above but with MOLLI scheme 4(1)3(1)2 (acquisition of 4, 3, and 2 images after the first, second, and third inversion pulse, respectively, with waiting periods of one heartbeat in between).[26]

For detailed patient characterization, cardiac MR also included LV function and LGE imaging in inspiratory breath-holding. For details, see the Supporting Information.

### Visual Analysis of Regional Myocardial Perfusion Deficits

The mid-ventricular DCE series acquired in diastole were analyzed visually for regional myocardial perfusion deficits, which were interpreted according to the American Heart Association (AHA) model by three readers (C.R., V.N., and U.R. with 4, 5, and 20 years of experience, respectively). The discrimination between perfusion deficits and possible dark rim artifacts was based on localization and duration of reduced SI increase during the first passage of CA as well as the presence of LGE visualized in postcontrast $T_1$ maps (Fig. 1).[3] In particular, an AHA segment was counted as a perfusion deficit segment if the majority of readers identified reduced SI increase in at least 50% along the subendocardial border of the segment.

### Determination of Regional Native $T_1$ Values

Systolic and diastolic global native myocardial and blood $T_1$ values were determined by manual segmentation of the endocardial and epicardial borders, as well as a region of interest (ROI) placed in the LV blood pool in the corresponding native $T_1$ maps by a reader with 4 years of experience (C.K.) using dedicated cardiac image analysis software (cvi[42], Circle Cardiovascular Imaging, Calgary, Canada). An offset of 25% from the drawn endo- and epicardial contours was chosen to ensure robust $T_1$ mean value estimates.[28] Moreover, diastolic $T_1$ maps were evaluated according to the six AHA segments of the measured mid-ventricular slice, halves of these AHA segments, thirds of these AHA segments, and quarters of these AHA segments to derive the corresponding 12-, 18-, and 24-sectional mean native $T_1$ values.

### Pixelwise and Regional MBF Determination

DCE series in end-systole (systolic DCE series) and diastasis (diastolic DCE series) together with an estimate of native myocardial and blood $T_1$ values were converted to pixelwise MBF maps and regional MBF estimates using in-house software implemented in MATLAB (MathWorks, Natick, MA). Figure 2 shows an overview of the image processing steps.

In a first step, the AIF was obtained from the DCE series as the mean signal from a central ROI in the LV blood pool, which was manually drawn onto one image of the perfusion series with suitable contrast between LV blood pool and myocardium, excluding papillary muscles. Then temporal SI changes of the AIF and every single pixel of the DCE series were converted to CA concentration changes using an SI model for the employed SR FLASH sequence[6,29]:

$$SI = c \cdot \left[ \left(1 - e^{-TD/T_1}\right) \cdot a^{n-1} + \left(1 - e^{-TR/T_1}\right) \cdot \frac{1 - a^{n-1}}{1 - a} \right] \quad \text{with } a = \cos(\alpha) \cdot e^{-TR/T_1} \tag{1}$$

where $\alpha$ denotes the flip angle, $TR$ the repetition time per phase encoding, $n$ the number of phase encoding steps between acquisition

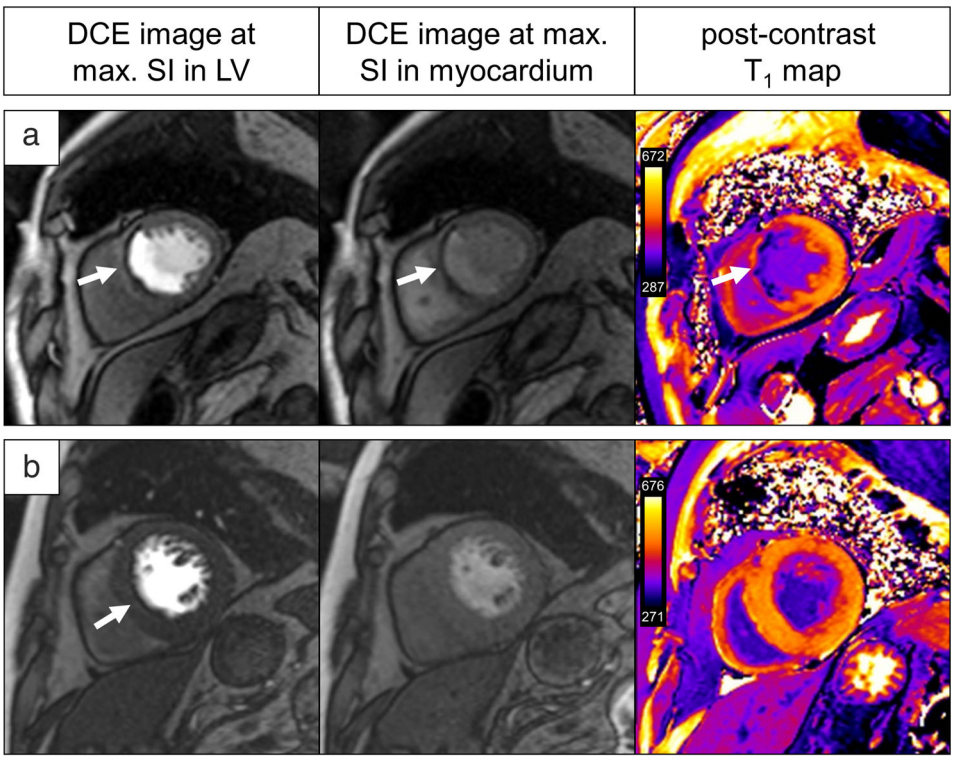


**FIGURE 1: Example of a perfusion deficit (a) and a dark rim artifact (b). In both cases, the DCE image during maximum SI in the LV (left panel) shows reduced SI increase in the myocardium (arrow). During maximum SI in the myocardium or equivalently some seconds later (center panel), only the perfusion deficit persists. Only the perfusion deficit demonstrates regional consistent late gadolinium enhancement in the postcontrast $T_1$ map (right panel). DCE = dynamic contrast-enhanced; SI = signal intensity; LV = left ventricle.**

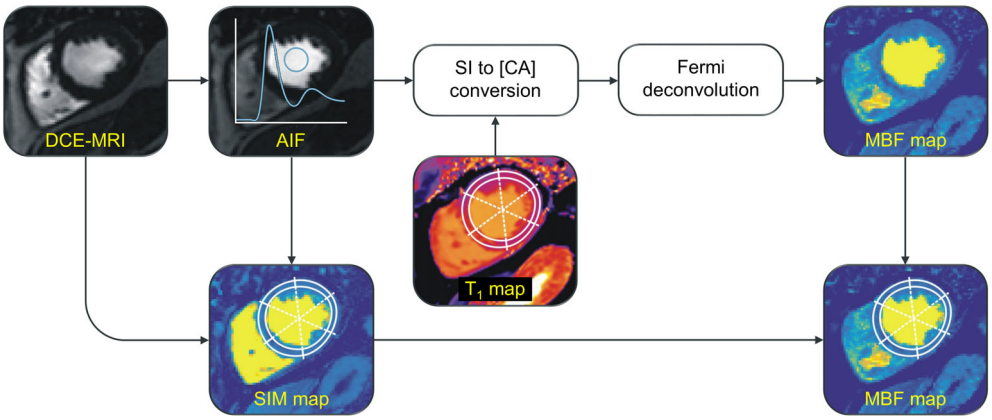


**FIGURE 2: Overview of the image processing steps for pixelwise and regional MBF quantification. The motion and coil sensitivity corrected perfusion MR data is first used to obtain the AIF from an ROI placed on one image with good contrast between LV blood pool and myocardium. Features of the extracted AIF are employed as temporal landmarks when generating a signal intensity maximum (SIM) map, which is used as a base image for the segmentation of the myocardium. The AIF and every single pixel of the perfusion series are converted from SI to CA concentration using SI model-based nonlinearity correction and incorporating native $T_1$ values measured from a precontrast $T_1$ map. Pixelwise MBF is determined employing Fermi function constrained deconvolution. DCE-MRI = dynamic contrast-enhanced magnetic resonance imaging; AIF = arterial input function; SI = signal intensity; CA = contrast agent; [CA] = contrast agent concentration; SIM = signal intensity maximum; MBF = myocardial blood flow; ROI = region of interest.**

start and *k*-space center (set to 31), and *TD* the time delay between the composite saturation pulse and the start of FLASH readout (set to 21.2 msec). *c* is a scaling factor proportional to the equilibrium magnetization and is assumed to be constant throughout the DCE series.[11] For every pixel, *c* was estimated employing the native $T_1$ value of blood or myocardium (for choices of native $T_1$ values, see next section) as well as the baseline signal determined as the temporal median of the signal from start to CA arrival in the LV blood pool. Equation 1 was then used to determine the $T_1$ values for each timepoint of the AIF and each pixel of the DCE series. CA concentrations corresponding to the calculated $T_1$ values were determined using the relationship:

$$\frac{1}{T_1} = \frac{1}{T_{1,0}} + r_1 \cdot [CA] \qquad (2)$$

where $T_{1,0}$ denotes the native $T_1$ estimate, $r_1$ the $T_1$ relaxivity constant of the contrast agent, and [CA] the contrast agent concentration. $r_1$ was set at 5.0 $L \cdot mmol^{-1} \cdot s^{-1}$ and assumed to remain unchanged when the CA passed from blood into tissue.[4,30]

Pixelwise MBF was quantified using Fermi function model constrained deconvolution, employing the AIF of the respective cardiac phase (eg, for DCE series in systole, the systolic AIF, which was converted to CA concentration with the systolic native $T_1$ value).[6] In doing so, the DCE series was restricted to the first passage of CA, with the end of the first passage identified as the valley point after the maximum of the AIF. The time shift between AIF and myocardial signal was identified as the one yielding the minimal fitting error between the deconvolution-determined and measured myocardial signal.[31] Global and segmental MBF values were calculated as the mean MBF of all pixels of the corresponding myocardial region; without further specification, MBF refers to global MBF.

### Experiments on the Impact of Native $T_1$ Values on MBF

At the SI-to-CA-concentration conversion processing step, several experiments were performed to evaluate the influence of native $T_1$ values on pixelwise MBF estimates. MBF maps were determined:

1. without nonlinearity correction (by only subtracting the baseline SI),
2. using ranges of native blood and myocardial $T_1$ normal values at 3T as well as the study population-averaged native blood and global myocardial $T_1$ values,[32–36]
3. employing individual patients' native blood and global myocardial $T_1$ values,
4. for the perfusion series in the systolic and diastolic phase, one time using native $T_1$ values of the respective cardiac phase and one time using the native $T_1$ values of the other cardiac phase,
5. using successively smaller native myocardial $T_1$ regions, ranging from six AHA segments of the mid-ventricular slice up to 24 sections.

Apart from the cardiac phase comparisons (experiment 4), all evaluations were performed employing diastolic DCE series. In experiments 3 and 5, diastolic native $T_1$ values were used. Additionally, the impact of the cardiac phase in which the AIF was measured was investigated by applying the systolic AIF to diastolic DCE series in experiments 1–4.

### Statistical Analysis

Statistical analysis was performed with MedCalc (MedCalc Software, Ostend, Belgium), considering $P < 0.05$ as significant. Mean values are specified together with standard deviations.

Equality of variances of distributions of perfusion and $T_1$ parameters was tested by the variance ratio test, their normality by the Kolmogorov–Smirnoff test. Study population mean values of

perfusion and $T_1$ parameters were compared by paired *t*-test or by Wilcoxon test, in case of nonnormality of the differences. Differences between perfusion and $T_1$ parameters in AHA segments with and without perfusion deficits were analyzed by means of unpaired *t*-test, Welch test, in case of unequal variances, or Mann–Whitney test, in case of nonnormality. Relationships between MBF and $T_1$ parameters were analyzed by the Pearson correlation coefficient ($r$) and its significance level. Relationships between global, segmental, and pixelwise MBF parameters derived by different methods were studied again by Pearson correlation analysis as well as linear regression and Bland–Altman analysis.

## Results

### Study Population

Demographic as well as LV function parameters of the study population are summarized in Supporting Information Table S1.

Whereas systolic and diastolic native blood $T_1$ values (1897 ± 138 msec vs. 1891 ± 136 msec) did not differ significantly ($P = 0.07$), systolic and diastolic global native myocardial $T_1$ values (1249 ± 65 msec vs. 1259 ± 80 msec) differed ($P < 0.05$). However, systolic and diastolic native $T_1$ values correlated strongly ($r = 1.00$ for blood and $r = 0.99$ for myocardium, $P < 0.05$ in both cases).

Myocardial perfusion deficits were identified in seven patients and 13 AHA segments; except for one AHA segment, this was agreed upon by all three observers. All perfusion deficits were surrounded by LGE (for further details, see Supporting Information). Mean diastolic native $T_1$ values in myocardial segments with perfusion deficits were significantly higher than in segments without perfusion deficits (1425 ± 170 msec vs. 1235 ± 66 msec, $P < 0.05$).

### MBF Quantification Without Subject-Specific Native $T_1$ Values

MBF determined without nonlinearity correction was significantly higher than MBF determined using subject-specific global native $T_1$ values (MBF SI = 0.71 ± 0.11 mL/(min·g) vs. MBF subject-specific $T_1$ = 0.61 ± 0.13 mL/(min·g), $P < 0.05$) and they correlated strongly ($r = 0.85$, $P < 0.05$).

Using the range of native myocardial and blood $T_1$ normal values for MBF estimation yielded lower mean MBF for higher native myocardial $T_1$ values and higher mean MBF for higher native blood $T_1$ values (Fig. 3a,b). Figure 3c,d

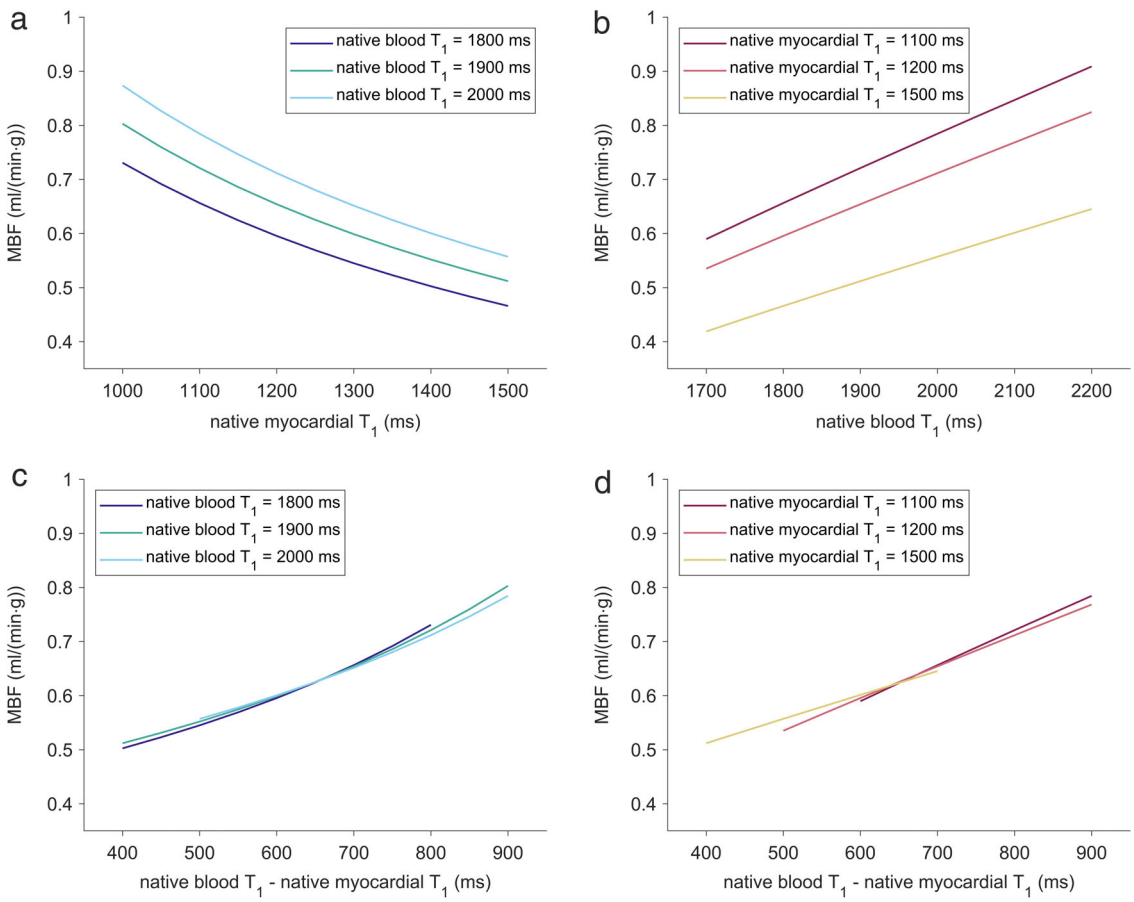


**FIGURE 3: MBF determined using normal ranges of native blood and myocardial $T_1$ values at 3T. The mean of MBF of all patients at varying myocardial $T_1$ values while keeping the blood $T_1$ value fixed (a) and at varying blood $T_1$ values while keeping the myocardial $T_1$ value fixed (b). The mean of MBF of all patients at varying differences between blood and myocardial $T_1$ values while keeping the blood $T_1$ value fixed (c) and while keeping the myocardial $T_1$ value fixed (d). MBF = myocardial blood flow.**

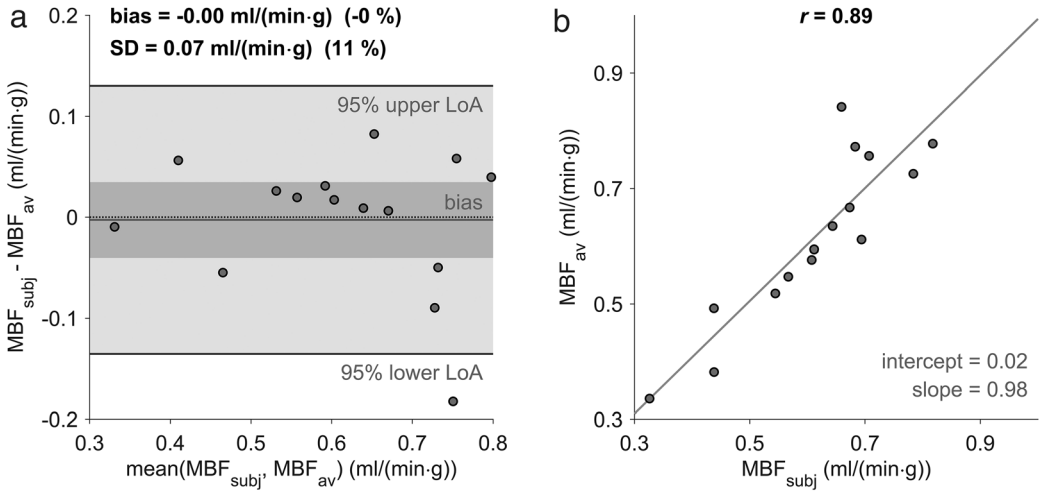


**FIGURE 4: Bland–Altman (a) and linear regression (b) plots for comparison of MBF estimates determined with subject-specific native $T_1$ values and the study population-averaged native $T_1$ values. The dark gray bar indicates the 95% confidence limits of the bias. MBF = myocardial blood flow; $MBF_{subj}$ = MBF with subject-specific native $T_1$ values; $MBF_{av}$ = MBF with study population-averaged native $T_1$ values; SD = standard deviation of differences; LoA = limits of agreement; $r$ = Pearson correlation coefficient.**

demonstrate that mean MBF becomes higher predominantly with the difference of native blood and myocardial $T_1$ values, irrespective of absolute blood or myocardial $T_1$ values. The mean MBF determined with the study population-averaged diastolic native $T_1$ values resulted in $0.62 \pm 0.15$ mL/(min·g). Whereas this mean value did not differ from the mean MBF determined with subject-specific native $T_1$ values ($P = 0.88$) and MBF estimates correlated strongly ($r = 0.89$, $P < 0.05$), MBF values of single patients deviated substantially from the mean difference (Fig. 4).

Of note, whereas mean MBF estimates were lower for higher native myocardial $T_1$ normal values and lower native blood $T_1$ normal values, the subject-specific MBF values did not correlate significantly either with the subject-specific native myocardial ($r = 0.26$, $P = 0.35$) or blood $T_1$ values ($r = 0.12$, $P = 0.64$) or their difference ($r = 0.04$, $P = 0.88$).

### *MBF Quantification With Systolic and Diastolic Native $T_1$ Values*

Systolic MBF determined using systolic native myocardial and blood $T_1$ values did not differ significantly from diastolic MBF determined with diastolic native myocardial and blood $T_1$ values (systolic MBF with systolic $T_1 = 0.59 \pm 0.14$ mL/(min·g) vs. diastolic MBF with diastolic $T_1 = 0.61 \pm 0.13$ mL/(min·g), $P = 0.12$). Moreover, a strong correlation between systolic and diastolic MBF estimates was observed (Fig. 5). However, MBF estimates calculated from native $T_1$ values at different cardiac phases differed significantly (systolic MBF with systolic $T_1 = 0.59 \pm 0.14$ mL/(min·g) vs. systolic MBF with diastolic $T_1 = 0.58 \pm 0.14$ mL/(min·g), $P < 0.05$; diastolic MBF with systolic $T_1 = 0.62 \pm 0.13$ mL/(min·g) vs. diastolic MBF with diastolic $T_1 = 0.61 \pm 0.13$ mL/(min·g), $P < 0.05$). Bland–Altman and regression plots of the comparisons are given in Fig. 6.

The maximum values of systolic and diastolic AIFs were not significantly different, either for SI curves (systolic $AIF_{max} = 663 \pm 194$ vs. diastolic $AIF_{max} = 657 \pm 187$, $P = 0.53$) or for CA concentration signals (systolic $AIF_{max} = 3.72 \pm 1.14$ mmol/L vs. diastolic $AIF_{max} = 3.67 \pm 1.13$ mmol/L, $P = 0.64$). Correspondingly, using the systolic AIF instead of the AIF of the respective cardiac phase did not change the results of the global MBF comparisons above (MBF SI vs. MBF subject-specific $T_1$, MBF study population-averaged $T_1$ vs. MBF subject-specific $T_1$, systolic MBF vs. diastolic MBF, systolic MBF with systolic $T_1$ vs. systolic MBF with diastolic $T_1$, diastolic MBF with diastolic $T_1$ vs. diastolic MBF with systolic $T_1$).

### *MBF Quantification Using Regional Native Myocardial $T_1$ Values*

Global MBF estimates determined with global native myocardial $T_1$ values did not differ significantly from global MBF estimates determined with AHA-segmental (6-segmental) native myocardial $T_1$ values (MBF global $T_1 = 0.61 \pm 0.13$ mL/(min·g) vs. MBF 6-segmental $T_1 = 0.61 \pm 0.13$ mL/(min·g), $P = 0.11$). The comparison of all 6-segmental MBF values calculated with global and 6-segmental native myocardial $T_1$ values also did not yield a significant difference ($P = 0.44$; Fig. 7a). However, if the segments without and with perfusion deficits were considered individually, a significant difference between 6-segmental MBF estimates determined with global and 6-segmental native myocardial $T_1$ values was observed: Segments without perfusion deficits showed higher MBF when 6-segmental instead of global

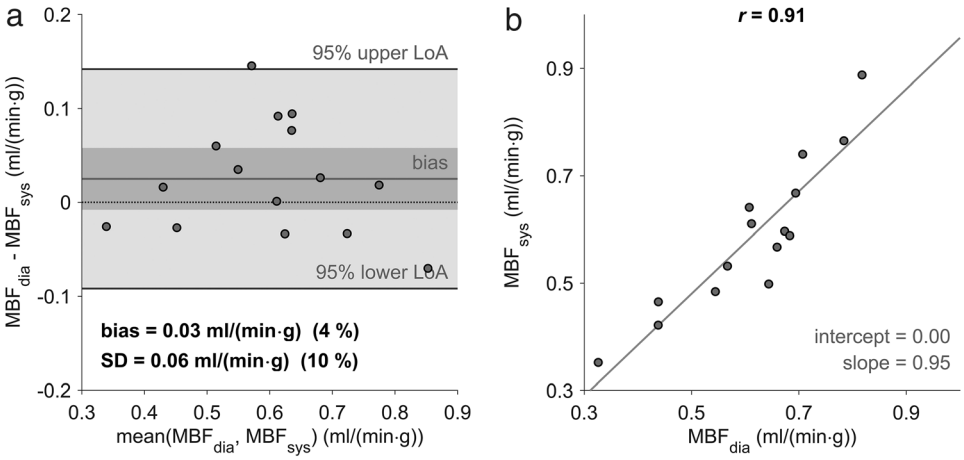


**FIGURE 5: Bland–Altman (a) and linear regression (b) plots for comparison of systolic and diastolic MBF estimates determined with systolic and diastolic native $T_1$ values, respectively. The dark gray bar indicates the 95% confidence limits of the bias. MBF = myocardial blood flow; $MBF_{dia}$ = diastolic MBF with diastolic native $T_1$ values; $MBF_{sys}$ = systolic MBF with systolic native $T_1$ values; SD = standard deviation of differences; LoA = limits of agreement; *r* = Pearson correlation coefficient.**

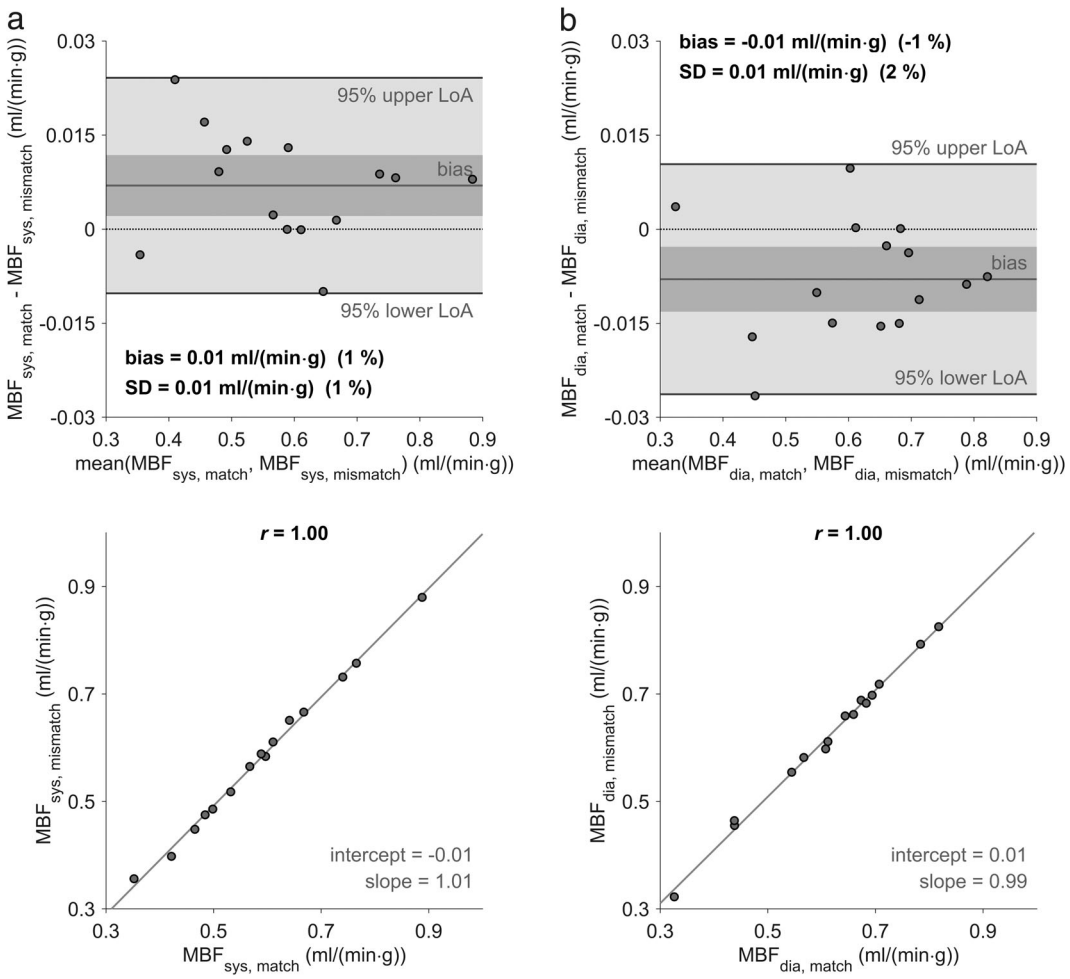


**FIGURE 6: Bland–Altman and linear regression plots for comparison of systolic (a) and diastolic (b) MBF estimates determined with native $T_1$ values of the respective cardiac phase and native $T_1$ values of the other cardiac phase. The dark gray bar indicates the 95% confidence limits of the bias. MBF = myocardial blood flow; $MBF_{sys, match}$ = systolic MBF with systolic native $T_1$ values; $MBF_{sys, mismatch}$ = systolic MBF with diastolic native $T_1$ values; $MBF_{dia, match}$ = diastolic MBF with diastolic native $T_1$ values; $MBF_{dia, mismatch}$ = diastolic MBF with systolic native $T_1$ values; SD = standard deviation of differences; LoA = limits of agreement; *r* = Pearson correlation coefficient.**

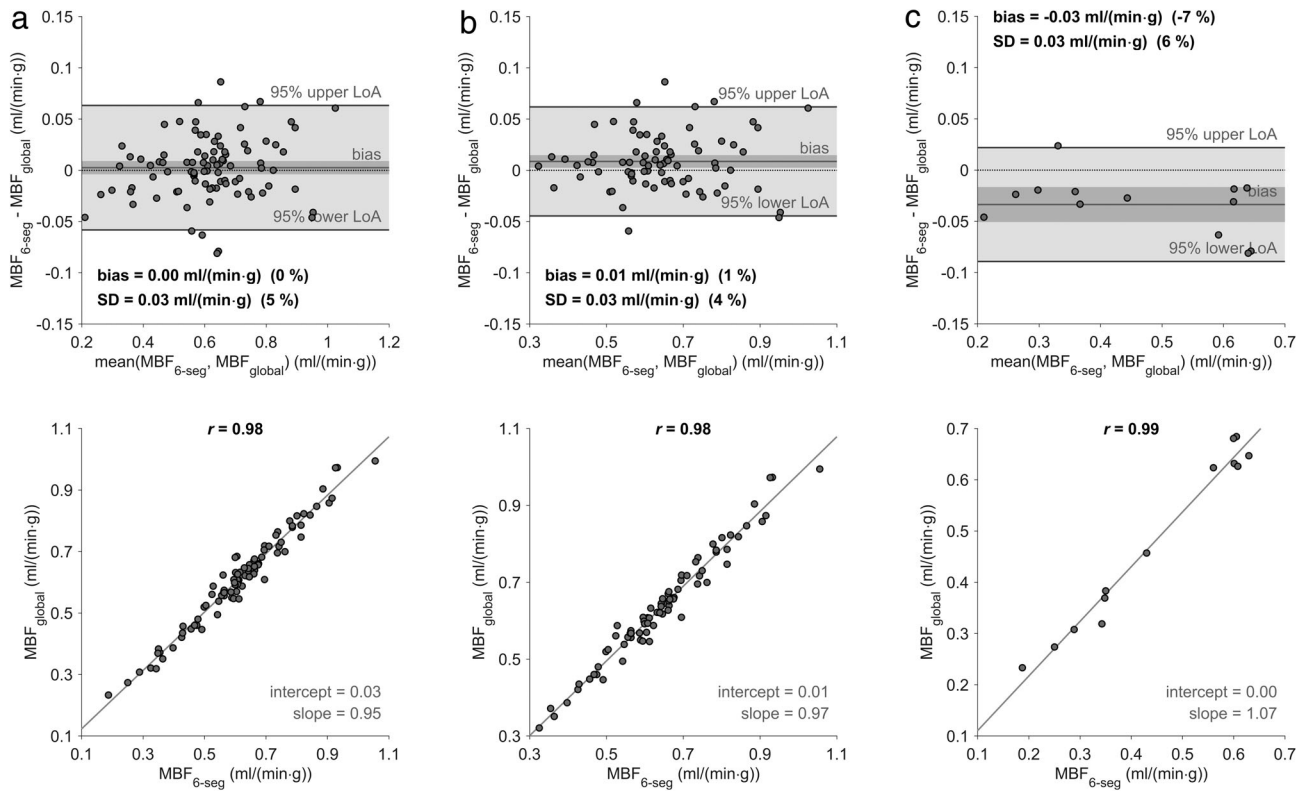


**FIGURE 7: Bland–Altman and linear regression plots comparing 6-segmental mean MBF values determined with global and 6-segmental native myocardial $T_1$ values. MBF of all segments of all patients (a), all segments without perfusion deficits (b), and all segments exhibiting perfusion deficits (c). The dark gray bar indicates the 95% confidence limits of the bias. MBF = myocardial blood flow; $MBF_{global}$ = MBF with global native $T_1$ values; $MBF_{6\text{-}seg}$ = MBF with 6-segmental native $T_1$ values; SD = standard deviation of differences; LoA = limits of agreement; *r* = Pearson correlation coefficient.**

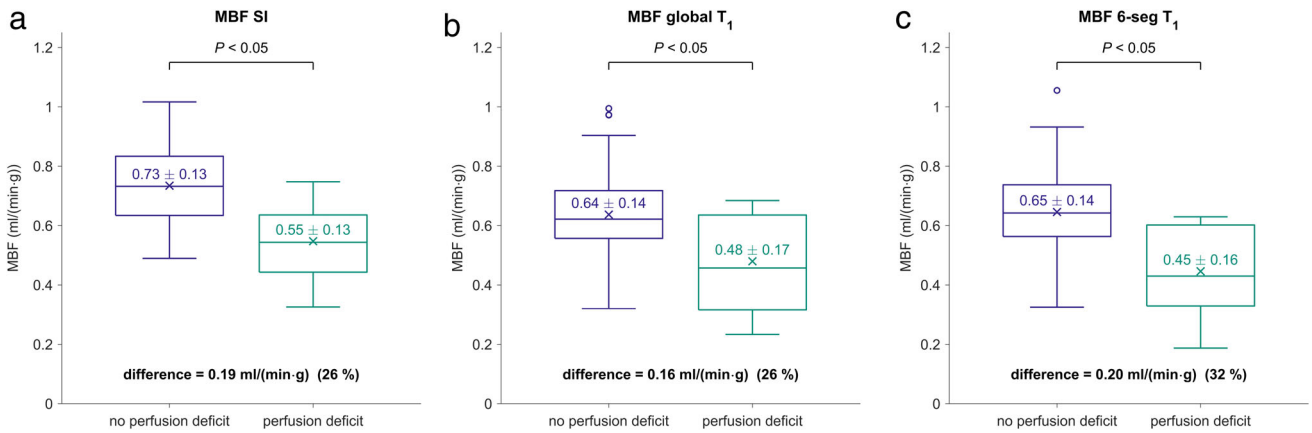


**FIGURE 8: Boxplots of MBF in segments with and without perfusion deficits, calculated without nonlinearity correction (a), with global native $T_1$ values (b), and with 6-segmental native $T_1$ values (c). Mean MBF is indicated by × and stated with the standard deviation, *P* refers to the comparison of the means. MBF = myocardial blood flow; MBF SI = MBF without nonlinearity correction; MBF global $T_1$ = MBF with global native $T_1$ values; MBF 6-seg $T_1$ = MBF with 6-segmental native $T_1$ values.**

native myocardial $T_1$ values were used ($P < 0.05$; Fig. 7b), while segments with perfusion deficits exhibited lower MBF ($P < 0.05$; Fig. 7c).

Figure 8 demonstrates boxplots of MBF estimates in segments with and without perfusion deficits, calculated without nonlinearity correction, with global native $T_1$ values and with 6-segmental native $T_1$ values. MBF in segments with perfusion deficits was significantly lower than MBF in segments without perfusion deficits in all cases. However, the mean difference of MBF between segments with and without perfusion deficits was smaller in the case of MBF calculated with global native $T_1$ and larger in the case of 6-segmental

**TABLE 1. Comparisons of Pixelwise MBF Values of All Patients Determined With a Successively Larger Number of Native Myocardial $T_1$ Sections**

| Comparisons of pixelwise MBF | *r* | Difference of MBF (mL/(min·g)) | *P* value |
|---|---|---|---|
| Global $T_1$ vs. 6-segmental $T_1$ | 0.99 | 0.0015 ± 0.0306 (0.25 ± 5.05%) | <0.05 |
| 6-segmental $T_1$ vs. 12-sectional $T_1$ | 1.00 | 0.0012 ± 0.0159 (0.19 ± 2.61%) | <0.05 |
| 12-sectional $T_1$ vs. 18-sectional $T_1$ | 1.00 | 0.0004 ± 0.0141 (0.07 ± 2.32%) | 0.33 |
| 18-sectional $T_1$ vs. 24-sectional $T_1$ | 1.00 | 0.0002 ± 0.0114 (0.04 ± 1.87%) | 0.10 |

*r* indicates the Pearson correlation coefficient; *P* value refers to Wilcoxon test.

native $T_1$ when comparing to MBF determined without nonlinearity correction. Comparisons of pixelwise MBF values determined with a successively larger number of native myocardial $T_1$ sections revealed that the largest impact of $T_1$-sectioning occurs from global to 6-segmental, considering the pixelwise MBF correlations and standard deviations of pixelwise differences (Table 1).

## Discussion

The main findings of this study are 1) pixelwise MBF quantification using native $T_1$ mapping for SI model-based nonlinearity correction is feasible; 2) using native $T_1$ normal values for blood and myocardium may lead to large variations in MBF estimates; 3) the cardiac phase in which native $T_1$ values are acquired significantly affects MBF estimates, even though the resulting MBF bias is small; and 4) MBF should be determined using regional instead of global native $T_1$ values.

### *Pixelwise MBF Quantification*

While previous studies on pixelwise MBF estimation in humans either used SI nonlinearity correction at image acquisition or employed native $T_1$ normal values for the SI model, the present study determined pixelwise MBF employing a clinical DCE protocol in combination with routinely acquired subject-specific native $T_1$ maps for SI model-based nonlinearity correction.[9,19,37] Both the average global MBF value of our study population and the mean MBF value in segments without perfusion deficits were within the range of published rest perfusion estimates (0.51 mL/(min·g) to 1.03 L(min·g)), which shows that the employed SI nonlinearity correction method yields reasonable MBF estimates.[9, 9,37] The comparably low MBF values of the present study can be explained by chronic CHD patients being very likely to exhibit (globally) reduced myocardial perfusion even at rest.

### *MBF Quantification Without Subject-Specific Native $T_1$ Values*

As observed previously, MBF estimates determined without nonlinearity correction were significantly higher than those determined using SI model-based nonlinearity correction with subject-specific native $T_1$ values.[19] Interestingly, employing native $T_1$ normal values in nonlinearity correction (experiment 2) might result in an even higher MBF bias.

Experiment 2 also showed that variations in native myocardial and blood $T_1$ values have a similarly strong effect on MBF estimates. It is therefore necessary to measure both native myocardial and blood $T_1$ values subject-wise instead of using fixed native $T_1$ reference values. This is further supported by the large limits of agreement in the Bland–Altman plot comparing MBF estimates determined with the study population-averaged native $T_1$ values and subject-specific native $T_1$ values.

### *MBF Quantification With Systolic and Diastolic Native $T_1$ Values*

Although the study population's mean MBF was lower in systole, this difference did not reach statistical significance because of the comparably large standard deviation of differences. This lack of phasic variation of MBF is in accordance with previous rest perfusion experiments.[38,39]

Experiment 4 implies that a bias is introduced if native $T_1$ values are not measured in the same cardiac phase as the perfusion series, which seems to be a direct consequence of the slightly different but strongly correlating systolic and diastolic native $T_1$ values. However, since the corresponding bias and standard deviation of differences were rather small compared to the systolic-to-diastolic MBF variation and even more to MBF differences between segments with and without perfusion deficits, it seems reasonable to measure native $T_1$ values in only one cardiac phase. Moreover, extrapolating from the mid-ventricular short-axis slice to the whole LV, the order of acquisition of slices in a clinical perfusion study, typically acquiring slices in different cardiac phases, should not play an essential role for MBF quantification.

Previous perfusion studies performing cardiac phase comparisons used the same systolic or diastolic AIF for MBF calculation to avoid potential AIF-dependent effects.[38,39] The present study found no significant differences between MBF estimates determined using the same systolic AIF and MBF estimates determined using AIFs of the corresponding cardiac phases. Moreover, in contrast to MBF studies on healthy volunteers, the present study did not find that $AIF_{max}$ was consistently lower in either systole or diastole.[38,40]

### *MBF Quantification Using Regional Native Myocardial $T_1$ Values*

Whereas there was no significant intersubject correlation between native myocardial $T_1$ and global MBF values, MBF estimates tend to be lower if the native myocardial $T_1$ values used for MBF estimation are higher (experiment 2). Consequently, MBF values of segments with perfusion deficits are overestimated and MBF values of segments without perfusion deficits are underestimated when using global instead of 6-segmental native myocardial $T_1$ values for nonlinearity correction. Moreover, while visually detected perfusion deficit segments demonstrated lower MBF values, irrespective of the employed native $T_1$ values, the MBF difference between segments with and without perfusion deficits was largest in the case of MBF calculated with 6-segmental native $T_1$ values. It is therefore appropriate to measure native myocardial $T_1$ values regionally in at least six segments to analyze possible perfusion deficits. Experiment 5 demonstrates that further $T_1$-sectioning of the myocardium leads to a reduced effect on pixelwise MBF estimates.

## Limitations

First of all, the patient number of the study was small and no healthy controls were investigated. Perfusion imaging was performed at rest only. However, since more than a third of the patients exhibited a rest perfusion deficit, a proof of principle was feasible without stress perfusion data. Findings on the influence of native $T_1$ values on MBF estimates can be expected to also hold for stress perfusion experiments. The use of positron emission tomography (PET) perfusion imaging as a gold standard comparison was not feasible. However, the global MBF estimates obtained were in accordance with the results of other MR rest perfusion studies.

Only images at the same mid-ventricular location were acquired, which was necessary for assessing the impact of systole and diastole on native $T_1$ values and MBF estimates. However, it can be assumed that the main findings of the present study would apply to basal and apical short-axis slices as well.

The MOLLI sequence is known to underestimate the $T_1$ value; nevertheless, it was chosen for native $T_1$ mapping due to its robustness and high signal-to-noise ratio.[26] Furthermore, the presence of a small native $T_1$ bias in all patients would not change the main findings of this study.

## Conclusion

Whereas cardiac phase-specific native $T_1$ values have a minor impact on MBF estimates, subject-specific and myocardial segment-specific native $T_1$ values substantially affect MBF quantification.

## Acknowledgment

The authors thank Ada Muellner, MS, for editing the article.

## References

1. McMurray JJV, Anker SD, Auricchio A, et al. ESC Guidelines for the diagnosis and treatment of acute and chronic heart failure 2012. Eur J Heart Fail 2012;14:803-869.
2. Bairey Merz CN, Pepine CJ, Walsh MN, et al. Ischemia and no obstructive coronary artery disease (INOCA). Circulation 2017;135:1075-1092.
3. Gerber BL, Raman SV, Nayak K, et al. Myocardial first-pass perfusion cardiovascular magnetic resonance: History, theory, and current state of the art. J Cardiovasc Magn Reson 2008;10:18.
4. Jerosch-Herold M. Quantification of myocardial perfusion by cardiovascular magnetic resonance. J Cardiovasc Magn Reson 2010;12:57.
5. Utz W, Niendorf T, Wassmuth R, Messroghli D, Dietz R, Schulz-Menger J. Contrast–dose relation in first-pass myocardial MR perfusion imaging. J Magn Reson Imaging 2007;25:1131-1135.
6. Jerosch-Herold M, Wilke N, Stillman AE, Wilson RF. Magnetic resonance quantification of the myocardial perfusion reserve with a Fermi function model for constrained deconvolution. Med Phys 1998;25: 73-84.
7. Köstler H, Ritter C, Lipp M, Beer M, Hahn D, Sandstede J. Prebolus quantitative MR heart perfusion imaging. Magn Reson Med 2004;52: 296-299.
8. Gatehouse PD, Elkington AG, Ablitt NA, Yang G-Z, Pennell DJ, Firmin DN. Accurate assessment of the arterial input function during high-dose myocardial perfusion cardiovascular magnetic resonance. J Magn Reson Imaging 2004;20:39-45.
9. Kellman P, Hansen MS, Nielles-Vallespin S, et al. Myocardial perfusion cardiovascular magnetic resonance: Optimized dual sequence and reconstruction for quantification. J Cardiovasc Magn Reson 2017;19:43.
10. Vallée J-P, Lazeyras F, Kasuboski L, et al. Quantification of myocardial perfusion with FAST sequence and Gd bolus in patients with normal cardiac function. J Magn Reson Imaging 1999;9:197-203.
11. Larsson HBW, Fritz-Hansen T, Rostrup E, Søndergaard L, Ring P, Henriksen O. Myocardial perfusion modeling using MRI. Magn Reson Med 1996;35:716-726.
12. Cernicanu A, Axel L. Theory-based signal calibration with single-point T1 measurements for first-pass quantitative perfusion MRI studies. Acad Radiol 2006;13:686-693.
13. Hsu L-Y, Kellman P, Arai AE. Nonlinear myocardial signal intensity correction improves quantification of contrast-enhanced first-pass MR perfusion in humans. J Magn Reson Imaging 2008;27:793-801.
14. Broadbent DA, Biglands JD, Ripley DP, et al. Sensitivity of quantitative myocardial dynamic contrast-enhanced MRI to saturation pulse efficiency, noise and t1 measurement error: Comparison of nonlinearity correction methods. Magn Reson Med 2016;75:1290-1300.
15. Messroghli DR, Moon JC, Ferreira VM, et al. Clinical recommendations for cardiovascular magnetic resonance mapping of T1, T2, T2* and extracellular volume: A consensus statement by the Society for Cardiovascular Magnetic Resonance (SCMR) endorsed by the European

Association for Cardiovascular Imaging (EACVI). J Cardiovasc Magn Reson 2017;19:75.

16. Pärkkä JP, Niemi P, Saraste A, et al. Comparison of MRI and positron emission tomography for measuring myocardial perfusion reserve in healthy humans. Magn Reson Med 2006;55:772-779.
17. Biglands J, Magee D, Boyle R, Larghat A, Plein S, Radjenović A. Evaluation of the effect of myocardial segmentation errors on myocardial blood flow estimates from DCE-MRI. Phys Med Biol 2011;56:2423-2443.
18. Motwani M, Fairbairn TA, Larghat A, et al. Systolic versus diastolic acquisition in myocardial perfusion MR imaging. Radiology 2012;262: 816-823.
19. Miller CA, Naish JH, Ainslie MP, et al. Voxel-wise quantification of myocardial blood flow with cardiovascular magnetic resonance: Effect of variations in methodology and validation with positron emission tomography. J Cardiovasc Magn Reson 2014;16:11.
20. Wissmann L, Niemann M, Gotschy A, Manka R, Kozerke S. Quantitative three-dimensional myocardial perfusion cardiovascular magnetic resonance with accurate two-dimensional arterial input function assessment. J Cardiovasc Magn Reson 2015;17:108.
21. Papanastasiou G, Williams MC, Kershaw LE, et al. Measurement of myocardial blood flow by cardiovascular magnetic resonance perfusion: Comparison of distributed parameter and Fermi models with single and dual bolus. J Cardiovasc Magn Reson 2015;17:17.
22. Kawel N, Nacif M, Zavodni A, et al. T1 mapping of the myocardium: Intra-individual assessment of the effect of field strength, cardiac cycle and variation by myocardial region. J Cardiovasc Magn Reson 2012; 14:27.
23. Reiter U, Reiter G, Dorr K, Greiser A, Maderthaner R, Fuchsjäger M. Normal diastolic and systolic myocardial T1 values at 1.5-T MR imaging: Correlations and blood normalization. Radiology 2013;271: 365-372.
24. Messroghli DR, Walters K, Plein S, et al. Myocardial T1 mapping: Application to patients with acute and chronic myocardial infarction. Magn Reson Med 2007;58:34-40.
25. Xue H, Shah S, Greiser A, et al. Motion correction for myocardial T1 mapping using image registration with synthetic image estimation. Magn Reson Med 2012;67:1644-1655.
26. Kellman P, Hansen MS. T1-mapping in the heart: Accuracy and precision. J Cardiovasc Magn Reson 2014;16:2.
27. Xue H, Zuehlsdorff S, Kellman P, et al. Unsupervised inline analysis of cardiac perfusion MRI. In: Proceedings of the 12th International Conference on Medical Image Computing and Computer-Assisted Intervention – MICCAI, September 2009. London, UK. Berlin, Heidelberg: Springer; 2009, p 741–749.
28. Piechnik SK, Ferreira VM, Lewandowski AJ, et al. Normal variation of magnetic resonance T1 relaxation times in the human population at 1.5 T using ShMOLLI. J Cardiovasc Magn Reson 2013;15:13.
29. Brix G, Schad LR, Deimling M, Lorenz WJ. Fast and precise T1 imaging using a TOMROP sequence. Magn Reson Imaging 1990;8:351-356.
30. Rohrer M, Bauer H, Mintorovitch J, Requardt M, Weinmann H-J. Comparison of magnetic properties of MRI contrast media solutions at different magnetic field strengths. Invest Radiol 2005;40:715-724.
31. Zarinabad N, Hautvast GLTF, Sammut E, et al. effects of tracer arrival time on the accuracy of high-resolution (voxel-wise) myocardial perfusion maps from contrast-enhanced first-pass perfusion magnetic resonance. IEEE Trans Biomed Eng 2014;61:2499-2506.
32. Lee JJ, Liu S, Nacif MS, et al. Myocardial T1 and extracellular volume fraction mapping at 3 Tesla. J Cardiovasc Magn Reson 2011;13:75.
33. Puntmann VO, Voigt T, Chen Z, et al. Native T1 mapping in differentiation of normal myocardium from diffuse disease in hypertrophic and dilated cardiomyopathy. JACC Cardiovasc Imaging 2013;6:475.
34. Dabir D, Child N, Kalra A, et al. Reference values for healthy human myocardium using a T1 mapping methodology: Results from the International T1 Multicenter cardiovascular magnetic resonance study. J Cardiovasc Magn Reson 2014;16:69.
35. Weingärtner S, Meßner NM, Budjan J, et al. Myocardial T1-mapping at 3T using saturation-recovery: Reference values, precision and comparison with MOLLI. J Cardiovasc Magn Reson 2016;18:84.
36. Reiter G, Reiter C, Kräuter C, Fuchsjäger M, Reiter U. Cardiac magnetic resonance T1 mapping. Part 1: Aspects of acquisition and evaluation. Eur J Radiol 2018;109:223-234.
37. Weng AM, Ritter CO, Beer M, Hahn D, Köstler H. Quantitative pixelwise myocardial perfusion maps from first-pass perfusion MRI. Br J Radiol 2014;87:20130727.
38. Radjenovic A, Biglands JD, Larghat A, et al. Estimates of systolic and diastolic myocardial blood flow by dynamic contrast-enhanced MRI. Magn Reson Med 2010;64:1696-1703.
39. Motwani M, Kidambi A, Uddin A, Sourbron S, Greenwood JP, Plein S. Quantification of myocardial blood flow with cardiovascular magnetic resonance throughout the cardiac cycle. J Cardiovasc Magn Reson 2015;17:4.
40. Nchimi A, Mancini I, Broussaud TKY. Influence of the cardiac cycle on time–intensity curves using multislice dynamic magnetic resonance perfusion. Int J Cardiovasc Imaging 2014;30:1347-1355.